EPJ Web of Conferences **239**, 01038 (2020) https://doi.org/10.1051/epjconf/202023901038
ND2019

Double-differential cross section measurement with low threshold detector for proton production induced by several tens of MeV protons

Yuji Yamaguchi[1,*], *Toshiya* Sanami[2], *Yusuke* Koba[3], and *Yusuke* Uozumi[1]

[1]Kyushu University, 744 Motooka, Nishi-ku, Fukuoka 819-0395, Japan
[2]High Energy Accelerator Research Organization (KEK), Japan
[3]National Institutes for Quantum and Radiological Science and Technology, Japan

Abstract. We have developed a low threshold detector consisting of Bragg curve counter (BCC), two silicon-surface barrier detectors (SSDs) and BGO scintillator to obtain experimental double-differential cross section (DDX) data for low energy proton production. Since the BCC offers advantage of self particle identification capability and a few μm-thick entrance window, protons produced by nuclear reactions down to 1 MeV have been identified. The capability of the detector is demonstrated in measurements using 70-MeV protons. Measured spectra are compared with calculation results of intra-nuclear cascade (INC) plus evaporation models and nuclear data library.

1 Introduction

The double-differential cross section (DDX) data of particle production from an energetic proton-nucleus reaction are required to estimate spatial distributions of energy deposition and radiation damage in devices used for accelerator driven system and particle radiation therapy. Since the estimation is performed with not only experimental data but also a Monte-Carlo simulation code such as PHITS[1], it is necessary that nuclear reaction models have high predictive power for DDXs.

To describe the secondary particle emission, two-stage model, which consists of the intra-nuclear cascade (INC) model[2] and the generalized evaporation model (GEM)[3], is generally used for the proton-nucleus reactions up to several hundreds of MeV. The GEM describes low energy particle emission from an excited nucleus with considering Coulomb barrier after INC stage. For the application above, GEM predictions on neutron and alpha particle emission play an important role in terms of neutronics and material damage. To obtain the accurate prediction, the GEM should be tested using experimental data. Experimental data of proton emission are useful to test both light particle emission and Coulomb barrier. In recent studies[4, 5], the INC model followed by the GEM has been improved for the $(p,\ p'x)$ reactions on light to heavy targets below 100 MeV, which has brought the GEM accurate information on excited nucleus. Poor prediction, however, has been pointed out for low energy proton emission from a heavy target ($A \geq 120$) in Ref. [5]. Although a theoretical study on low energy proton emission has been starting to improve the GEM, few experimental DDX data are available for validating it. Thus, new series of experimental DDX data covering low energy range down to 2 MeV are highly demanded for wide range of target mass and angles.

In general, the measurement of DDX has been performed with $\Delta E - E$ method for particle identification using two silicon-surface barrier detectors (SSDs). In this method, the threshold energy with particle identification is limited by the thickness of the transmission SSD. Because 150-μm-thick SSD is commercially available as the thinnest SSD for the purpose of particle identification, most of the data taken with conventional SSDs have threshold energy around 4 MeV.

In this study, we develop a low threshold detector consisting of Bragg curve counter (BCC)[6, 7], two SSDs, and BGO scintillator to obtain the systematic DDX data covering low energy range. The BCC has advantages of the thin entrance window and self particle identification capability in low energy threshold measurements.

2 Low threshold detector

The schematic drawing of the low threshold detector is shown in Fig. 1. Particles produced by nuclear reactions enter the detector through the entrance window of the BCC.

The BCC is a parallel plate gas ionization chamber with a grid. The chamber is cylindrically shaped and sealed using O-rings to keep Ar + 10 % CH_4 gas as a counting gas. The gas pressure is variable up to 106.6 kPa (800 Torr). The electrodes of the BCC consist of the cathode, field shaping rings, grid, and anode. The distances from the cathode to the grid and from the grid to the anode are set to 150 mm and 5 mm, respectively. The cathode is a stainless-steel disk with a central hole 10 mm in diameter covered with a 2.2-μm-thick aluminized Mylar film and

*e-mail: yyamaguchi@nucl.kyushu-u.ac.jp

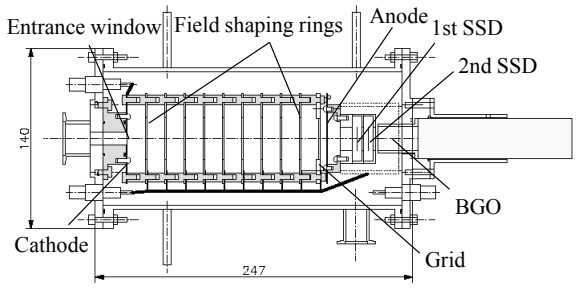

Figure 1. Schematic drawing of low threshold detector. Particles produced by nuclear reactions come from the left side of this drawing and pass through the entrance window.

tungsten wire mesh supporting the film. Because the aluminized surface and the stainless-steel disk are connected electrically, the cathode plays the role of a thin entrance window, which introduces charged particles with small energy loss. The field shaping rings and the grid are arranged at equal intervals and connected with a chain of 1 MΩ resistors to maintain a uniform electric field. The electric field is formed by providing high voltage for the cathode, field shaping rings and grid. The anode plate is a stainless-steel disk with a central hole 32 mm in diameter. The hole is covered with a 5-μm-thick aluminum foil which is connected with the stainless-steel disk electrically. Thus, the anode allows energetic charged particles to penetrate with small energy loss for the measurement using the BCC as a transmission detector, as will be described later.

The low energy charged particle stopped in front of the grid produces electron-ion pairs along its trajectory by ionizing the counting gas. Since the number of electrons is proportional to the energy deposited by the charged particle, distribution of electrons corresponds to Bragg curve. Keeping the distribution, the electrons drift toward the grid because of the electric field, and then all the electrons pass through the grid and reach the anode by setting electric field strength between the grid and the anode stronger than that between the cathode and the grid. In this case, time distribution of the anode signal has inverse shape of the original distribution of electrons (Fig. 2). Therefore, the energy (E_{BCC}) and the atomic number of the charged particle can be deduced from integral and peak height of the anode signal, respectively. The integral of the anode signal is obtained using a long time constant (6 μs) amplifier and the peak height a short time constant (0.25 μs) shaping amplifier. This particle identification method can be applied from 1 MeV to 3 MeV for protons using 106.6 kPa (800 Torr) counting gas.

To identify the energetic charged particle which penetrates the anode, $\Delta E - E$ method is applied using the BCC and backward detectors, where the BCC works as a transmission detector. The backward detectors of two SSDs and a BGO scintillator are placed inside the chamber. Because the thickness of the 1st SSD and the 2nd SSD are 400 μm and 1 mm, respectively, the combination of the BCC and the 1st SSD and that of SSDs can identify protons with 4 MeV to 7 MeV and 8 MeV to 15 MeV, respectively. The BGO scintillator with the thickness of 31 mm can stop all the particles with energy of interest.

3 Experiment

The experiment was performed at cyclotron facility of National Institute of Radiological Sciences (NIRS), Japan. The plan view of the experimental setup is shown in Fig. 3. A scattering chamber was connected directly to the beam duct of the cyclotron and evacuated to less than 10^{-3} Pa. Accelerated protons with energy of 70 MeV hit a thin film target located inside the scattering chamber and entered a Faraday cup consisting of a stainless-steel pipe and a graphite beam dump. The targets of $^{\mathrm{nat}}$C, ^{27}Al, $^{\mathrm{nat}}$Cu, $^{\mathrm{nat}}$Ag, $^{\mathrm{nat}}$Ta, and ^{197}Au were mounted on a target changer. Energy spectra of charged particles emitted from the target were measured at 60°, 120° and 150° in the laboratory system with the low threshold detector. The detector was operated at gas pressures of 53.3 kPa (400 Torr) and 106.6 kPa (800 Torr) to compensate a part of gaps in obtained spectra due to detector dead layers and electronics thresholds.

A typical example of low energy particle identification using the BCC is shown in Fig. 4. Charged particles with enough energy to form the Bragg peak are identified. For the high energy side of hydrogen, helium and lithium, particles penetrating through the anode are observed within dashed circles in Fig. 4. As mentioned in Sec. 2, these particles are identified applying the $\Delta E - E$ method.

The measured data were corrected to remove the effects of background component and energy loss in the tar-

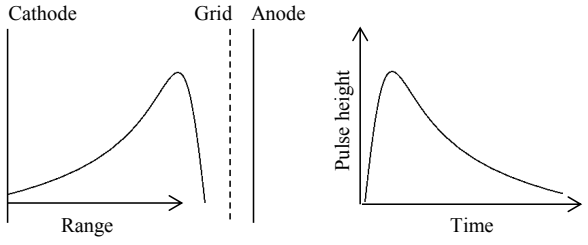

Figure 2. Distribution of electrons produced in BCC (left) and time distribution of anode signal (right). The polarity of the anode signal is inverted in this figure.

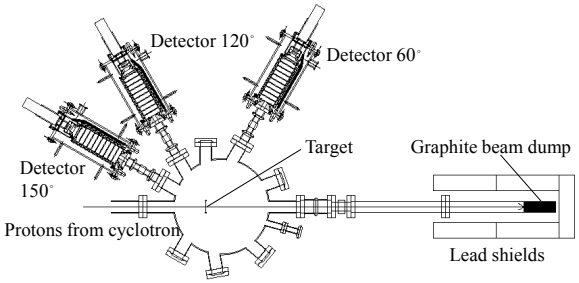

Figure 3. Plan view of experimental setup. Accelerated protons come from the left side of this view.

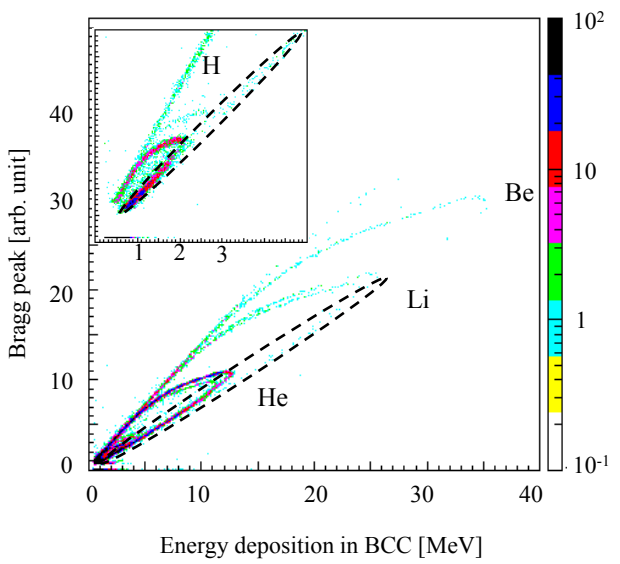

Figure 4. E_{BCC} vs Bragg peak height two-dimensional plot. The inset shows the plot in low energy region up to 5 MeV. The identified charged particles from H to Be are shown. Particles penetrating the anode are identified inside dashed circles.

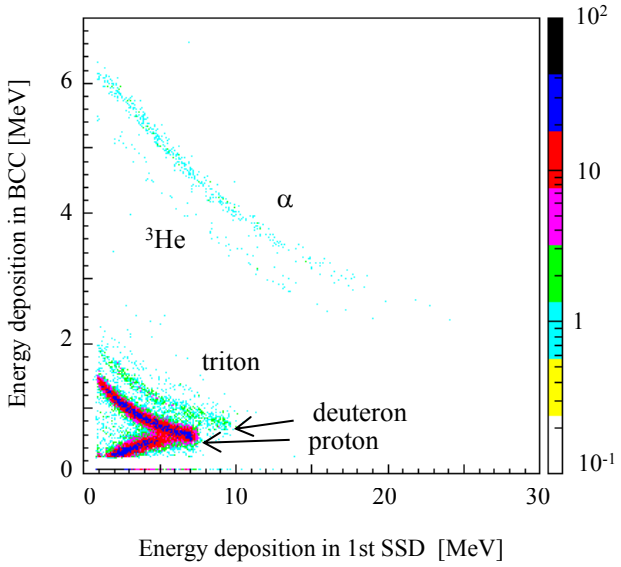

Figure 6. ΔE (BCC) vs E (1st SSD) two-dimensional plot. The identified particles of proton, deuteron, triton, ^{3}He and α are shown.

get, in the entrance window and in the anode. Finally, DDXs were obtained by

$$\frac{d^2\sigma}{d\Omega dE} = \frac{Y}{s\phi\Delta\Omega\Delta E}\,, \qquad (1)$$

where s is the number of target atoms per unit area, ϕ is the number of incident protons, $\Delta\Omega$ is the solid angle, ΔE is the energy bin width, and Y is the number of charged particles identified in ΔE. The solid angle $\Delta\Omega$ was determined by α-particle counting using ^{241}Am check source placed instead of the target.

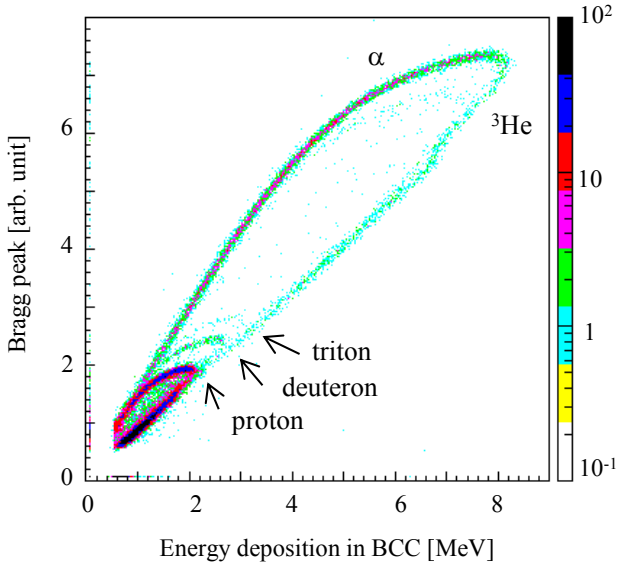

Figure 5. E_{BCC} vs Bragg peak height two-dimensional plot. The identified particles of proton, deuteron, triton, ^{3}He and α are shown.

4 Results and discussion

Figure 5 shows E_{BCC} vs Bragg peak height two-dimensional plot obtained using 53.3 kPa counting gas. In this figure, events having energy less than 8.5 MeV are shown to discuss self particle identification capability for hydrogen isotopes. In the energy range from 1 MeV to 3 MeV, the hydrogen isotopes of protons, deuterons and tritons are identified because the Bragg peak is characterized by the mass number of the charged particle as well as the atomic number. Since the separation between proton and deuteron is observed above 1 MeV in Fig. 5, the threshold energy of proton identification was determined to be 1 MeV.

Figure 6 shows ΔE (BCC) vs E (1st SSD) two-dimensional plot obtained using 53.3 kPa counting gas. The hydrogen isotopes are also identified in this figure because of good energy resolution of the BCC. Although

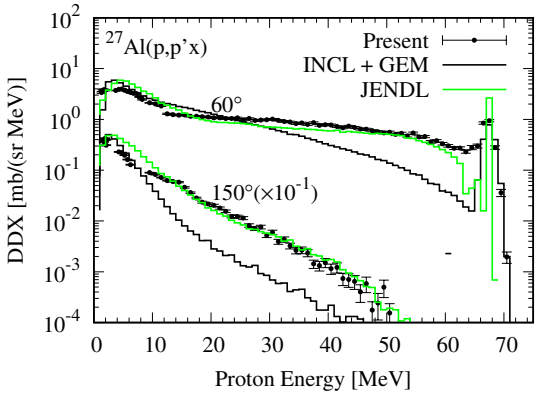

Figure 7. Measured and calculated proton spectra at 60° and 150° for 70-MeV incident protons on ^{27}Al. Circles: present data; black lines: INCL plus GEM results; green lines: JENDL results.

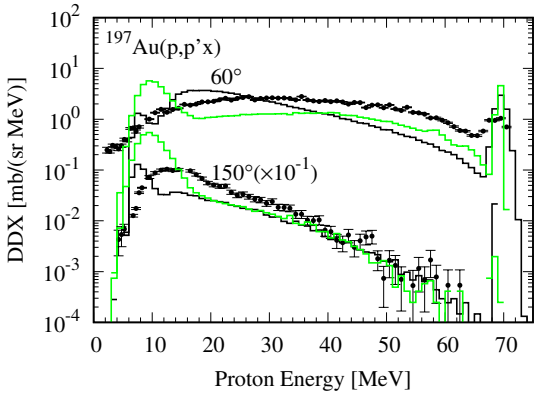

Figure 8. Measured and calculated proton spectra at 60° and 150° for 70-MeV incident protons on ^{197}Au. Circles: present data; black lines: INCL plus GEM results; green lines: JENDL results.

the identified proton line partially overlaps with folding back lines of hydrogen isotopes penetrating through the 1st SSD, the penetrating events can be removed analytically using the signal of the 2nd SSD.

Figures 7 and 8 show proton spectra at 60° and 150° for 70-MeV incident protons on ^{27}Al and ^{197}Au targets, respectively. The present data are shown with closed circles. Calculation results that were obtained using nuclear data library of JENDL-4.0/HE (green) and the INC plus GEM which is employed in the PHITS as the default model[8] (black) are shown with solid lines.

The measured spectra were obtained in a wide energy range and the threshold energy of 1.3 MeV was obtained because of the thin entrance window and self particle identification capability of the BCC. Below 10 MeV, measured spectra show a different tendency between ^{27}Al and ^{197}Au targets: the ^{27}Al$(p,\ p'x)$ spectra increase whereas the ^{197}Au$(p,\ p'x)$ spectra decrease as proton energy decreases, which reflects difference of Coulomb barrier.

The calculation results show reasonable agreement with measured spectra below 10 MeV for the ^{27}Al$(p,\ p'x)$ reaction, but, in contrast, they show disagreement with measured spectra for the ^{197}Au$(p,\ p'x)$ reaction as follows. INC plus GEM results have threshold at 6 MeV whereas measured data exist below 6 MeV. In addition, the peak energy of INC plus GEM results at 150° is lower than that of measured spectrum. JENDL spectra around 10 MeV are much larger than measured spectra because large level density is given to ^{196}Au.

5 Conclusion

We developed a low threshold detector consisting of the BCC, two SSDs, and BGO scintillator to obtain systematic DDX data covering low energy range for tens of MeV proton induced reactions. Using the detector, proton spectra with threshold energy of 1.3 MeV were obtained. The experimental results were compared with calculation results. Calculation results of JENDL and INC plus GEM are in reasonable agreement with measured spectra for the ^{27}Al target. For the ^{197}Au target, INC plus GEM results have threshold though measured data exist below the threshold. JENDL spectra around 10 MeV are much larger than measured spectra.

Acknowledgements

This work was conducted at Joint-use Research Facility for Collaborative Project with NIRS-Cyclotron.

References

[1] T. Sato et al., J. Nucl. Sci. Technol. **55**, 684 (2018)
[2] H. W. Bertini, J. Phys. Rev. **188**, 1711 (1969)
[3] S. Furihata and T. Nakamura, J. Nucl. Sci. Technol. **39**:sup2, 758 (2002)
[4] Y. Uozumi et al., Phys. Rev. C **86**, 034610 (2012)
[5] Y. Uozumi et al., J. Nucl. Sci. Technol. **52**, 264 (2015)
[6] T. Sanami et al., Nucl. Instr. and Meth. A **589**, 193 (2008)
[7] M. Hagiwara et al., Nucl. Instr. and Meth. A **592**, 73 (2008)
[8] A. Boudard et al., Phys. Rev. C **87**, 014606 (2013)